3,4-Dihydroxybenzoic acid removal from water by goethite modified natural sand column fixed-bed: experimental study and mathematical modeling

Hassan Ouachtak[a,b,*], Siham Akhouairi[c], Redouane Haounati[c], Abdelaziz Ait Addi[c], Amane Jada[d,e,*], Mohamed Labd Taha[a], Jamaa Douch[c]

[a]*Laboratoire de Chimie Appliquée & Environnement, Equipe Bio-organique Appliquée, Faculté des Sciences, Université Ibn Zohr, Agadir, Maroc, emails: ouachtakhassan@gmail.com (H. Ouachtak), labd999@gmail.com (M.L. Taha)*
[b]*Faculté des Sciences Appliquées Ait Melloul, Université Ibn Zohr, Agadir, Maroc*
[c]*Département de chimie, Faculté des Sciences, Université Ibn Zohr, Agadir, Maroc, emails: akhouairisiham@gmail.com (S. Akhouairi), haounati.redouane@gmail.com (R. Haounati), a_aitaddi@yahoo.fr (A.A. Addi), douch.791955@gmail.com (J. Douch)*
[d]*IS2M, CNRS-UHA, 15 Rue Jean Starcky, 68057 Mulhouse cedex, France, Tel. 0033 3 89608709; email: amane.jada@uha.fr (A. Jada)*
[e]*Université de Strasbourg, Strasbourg, F-67081, France*

ABSTRACT

In this paper, a continuous adsorption of 3,4-Dihydroxybenzoic acid (3,4-DHBA) has been studied by using goethite modified natural sand (GMNS) as adsorbent in a fixed-bed column. Scanning electron microscopy coupled with energy-dispersive X-ray analysis, X-ray diffraction and Fourier transform infrared spectroscopy (FTIR), characterized the GMNS surface. The effect of various experimental parameters including pH (5 and 9), flow rate (1, 2, and 3 mL/min) and initial 3,4-DHBA concentration (15, 40 and 60 mg/L) on the transport and adsorption of 3,4-DHBA onto the column were investigated in detail. The obtained result shows that exhaustion time decreased with increasing initial 3,4-DHBA concentration, flow rate and pH. The highest value of adsorbed amount q = 35.66 mg/Kg was obtained from injection of 60 mg/L of initial 3,4-DHBA concentration solution with flow rate, Q = 1 mL/min, at pH = 5 in column packed with GMNS. The Thomas and Yoon–Nelson models were applied to describe the breakthrough curves of adsorption of 3,4-DHBA onto GMNS solid. The linear regression analysis demonstrated that the Yoon–Nelson model fitted well with the column adsorption data for 3,4-DHBA. In addition, adsorption mechanism was proposed based on the results FTIR before and after adsorption. The GMNS adsorbent can be regenerated for three adsorption–desorption cycles using sodium hydroxide solution.

Keywords: 3,4-DHBA adsorption; Goethite modified natural sand; Column fixed-bed; Transport; Modeling

1. Introduction

3,4 dihydroxybenzoic acid (3,4-DHBA) is a phenolic compound containing both –COOH and –OH groups; it has been considered as a model molecule of natural organic matter (NOM) [1–5]. On the other hand, 3,4-DHBA is used in the pharmaceutical, cosmetics, rubber, oil industries, and food industries [6–8]; it is present in the wastewater discharged as industrial effluents [7,9,10]. The presence of 3,4-DHBA in the water causes problems such as color, taste, and odor. Besides, 3,4-DHBA can react with the added chlorine during disinfection and produce harmful organic compounds such as halo acetic acids and chloroform, which can cause liver, kidney or central nervous system problems [11–15]. Thus, 3,4-DHBA has strong complexation ability with divalent and trivalent metal ions in aqueous media and thus increases their transportation in waters and natural environments [16,17]. Additionally, 3,4-DHBA causes an increase in the chemical

---

* Corresponding authors.

oxygen demand in water and leads to a series of environmental problems [7,10]. The maximum level of 3,4-DHBA permitted in drinking water by environmental organizations in Canada, USA and European Economic Community are 2 μg/L [3,18]. For all these reasons, it is important to use removal methods of these compounds from water. Several techniques have been used to remove the phenolic acids from the water such as electrochemical oxidation [19], membrane filtration [20–22], photocatalysis [3,23,24], and coagulation-flocculation [25–27]. However, these techniques generate a large amount of sludge and they are high-cost and are not always adaptable as regards the efficiency of the elimination of the NOM of low molecular weight [7,13,28,29]. The adsorption process has been proven as a good technique for organic matter removal from aqueous solutions, and it is advantageous over other methods, due to its low-cost, easy separation in the treated water, economy, and simplicity [13,15,30–33].

A wide range of solid materials have been used to remove phenolic acids and NOM from water, including bio adsorbent [10,13,34], modified clay [35,36], graphite oxide [37] and activated carbon [12,14,38,39]. Among them, fresh activated carbon adsorption is one of the best materials utilized for the removal of NOM from aqueous solutions. However, this adsorbent is expensive, which makes it uses difficult for wastewater treatment, especially in developing countries. The goethite is a great adsorbent for the removal of organic matter of water due to its low operating cost and higher adsorption efficiency [33,40,41]. However, it is difficult to pack goethite nanoparticles in a fixed-bed column because it is hard to separate for regenerating and easy to be washed away [42]. The idea behind this work is to use goethite nanoparticle as a large adsorbent to remove organic matter from water in continuous systems (column adsorption). Nevertheless, it is difficult to condition the goethite nanoparticle in a fixed-bed column. For this, a support material is necessary to immobilize goethite in a fixed-bed test. Natural sand (NS) is an excellent choice for its low-cost, chemical stability and availability [43]. The goethite modified natural sand (GMNS) is an innovative tool to avoid the problem of using powdered goethite in continuous water treatment processes [44,45]. To date, no systematic studies were carried out to investigate the application of goethite coating on the sand surface for removing 3,4-DHBA from water in a fixed-bed test. In this study, GMNS prepared was used as an adsorbent for the removal of 3,4-DHBA fixed-bed experiments. Experimental factors such as pH, initial concentration and flow rate were investigated. The breakthrough curves for the transport of 3,4-DHBA were analyzed using two different models, Thomas and Yoon–Nelson models. The application of these semi-empirical models is to determine the adsorbed quantity of 3,4-DHBA in the goethite coated quartz sand column.

2. Materials and methods

2.1. Reagents

3,4-DHBA (Data are shown in Table 1) and sodium chloride (NaCl) were purchased by Sigma-Aldrich (France). The natural sand NS (grain size range = 50–350 μm) provided by 'quartz Alsace' company (France) and was used as a natural adsorbent in our previous studies [15,32,46]. The goethite nanoparticles employed in this work were purchased from BASF Company (Germany).
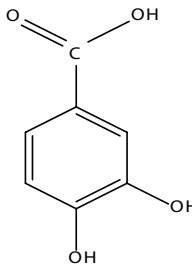
2.2. Preparation of adsorbent

In this present work, the adsorbent GMNS was prepared by the heterogeneous suspension reaction method where the goethite nanoparticles were mixed with the natural sand. Several authors [47–50] have described this method. Briefly, the natural sand quartz with a grain size range of 50–350 μm was cleaned with 1 M HCl for 24 h and then rinsed by deionized water to eliminate chemical impurities. The GMNS was obtained by shaking a suspension containing 25 g of goethite and 1,000 g of natural sand. Then, the mixture was agitated for 24 h at temperature 60°C. Finally, the modified sand by goethite was washed with deionized water until the runoff was clear, and then it was dried for 24 h. Fig. 1 summarizes the GMNS preparation steps.

2.3. Characterization

The GMNS were characterized by X-ray diffraction (XRD) using a Bruker AXS D-8 diffractometer using Cu-Ka radiation in Bragg–Brentano geometry (q–2q) (Bruker AXS GmbH Germany). The samples of GMNS before and after adsorption were characterized by Fourier transform infrared spectroscopy (FTIR) in the range of 4,000–400 cm^{-1} using an ABB Bomem FTLA 2000 spectrometer (Canada) with 16 cm^{-1} resolution. Scanning electron microscopy (SEM)

Table 1
3,4-DHBA properties [4]

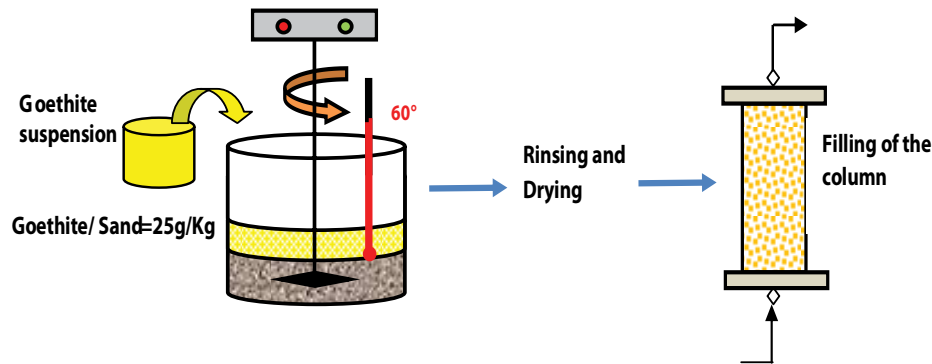| Full name	Chemical formula	Chemical structure	Molecular weight (g/mol)	pK$_a$	Solubility (g/L)	λ$_{max}$ (nm)
3,4, Dihydroxybenzoic Acid				4.22		
				8.67		
	$C_7H_6O_4$		154.11		20	260

Fig. 1. GMNS preparation steps.

micrographs were obtained on a FEI FEG 450 scanning electronic microscope (Mascir Laboratory, Morocco) at 120 kV. The elemental composition of the sample was confirmed by energy-dispersive X-ray analysis (EDAX).

2.4. Experimental device

The experimental device and the adsorption experiments used in this work were described in detail in our previous publication [5,15,46]. Briefly, dry GMNS (73 g) was packed into glass column made of Altuglas (internal diameter = 2.4 cm; bed length = 9.8 cm; density = of 1.64 g/cm³). The pore volume was between 17,5 and 19,5 mL. The porosity varied from 0.36 to 0.38 and the Peclet number remained always higher than 162.

The 3,4-DHBA concentration in the effluent was analyzed by a UV/visible spectrophotometer (Shimadzu UV-1800, Japan) at wavelength, λ = 260 nm. Also, the ionic strength of the 3,4-DHBA solutions was fixed by NaCl at 0.01 M, and this value corresponds to the ionic strength of the contaminated aquifers [51]. The initial pH of the solution was adjusted by 0.1 M NaOH or HCl solutions, and pH measurements were managed by using a pH meter (Model HANNA 210).

The adsorbed (M_{ads}) 3,4-DHBA mass at the mineral-water interface was determined by using Eq. (1): [47].

$$\left(M_{3,4DHBA}\right)_{ads} = \sum_i \left(\left(C_0 - C_i\right)V_i - C_i V_p\right) \qquad (1)$$

C_0 is the initial concentration of organic compounds injected, C_i and V_i are respectively the concentration and the volume of the fraction i, collected at the outlet of the column; V_p is the total volume of pores. Practically, the mass balances were calculated as the difference between the breakthrough data of the conservative tracer KI and 3,4 DHBA for each experiment and both the adsorption fronts.

The adsorbed amount of the column was evaluated using the following Eq. (2):

$$q\left(mg/Kg\right) = \frac{\sum_i \left(\left(C_0 - C_i\right)V_i - C_i V_p\right)}{m} \qquad (2)$$

where m (Kg) is the mass of adsorbent in the column.

Transport and adsorption experiments, the influence of pH (pH = 5 and pH = 9) flow rate Q (Q = 1, 2, and 3 mL/min),

initial 3,4 DHBA concentration (C_0 = 15, 30 and 60 mg/L) on the adsorption of 3,4-DHBA onto column GMNS column were investigated by comparing the breakthrough curves. It should be emphasized that in all column experiments, the breakthrough curves are obtained by plotting (C/C_0) vs. time (t).

3. Results and discussion

3.1. Characterization of GMNS

3.1.1. Scanning electron microscopy - energy-dispersive X-ray analysis

The SEM images of GMNS (Figs. 2a and b) show that the sand surface is not completely covered by the goethite particles. A few goethite particles are deposited on the sand surface in agglomerate form, which gives the surface non-uniform splicing. Besides, Fig. 2b shows typical acicular needle-shaped deposed particles specific to formed the goethite.

The EDAX analyses for GMNS (Fig. 2c) confirm the deposition of goethite by the presence of Fe peaks at the surface of goethite coated quartz sand. The EDAX spectrum also showed the presence of other major elements (silicon Si, and oxygen O).

3.1.2. XRD of GMNS

The XRD pattern of Goethite, GMNS, and NS are shown in Fig. 3. The XRD pattern of GMNS consists essentially of quartz SiO_2 and Goethite. The values of 2θ values = 20.99°, 26.77° and 50.45° correspond to the diffraction of quartz SiO_2 (JCPDS-No. 89-1961) and the peaks at 2θ values 21.27, 36.71 and 55.12 were ascribed to the diffraction of goethite (JCPDS - No.29-0713).

3.1.3. Fourier transform infrared spectroscopy

The surface functional groups of GMNS and NS were determined by FTIR. The FTIR absorption spectrum is shown in Fig. 4.

The FTIR spectrum of the GMNS and NS exhibited similar bands:

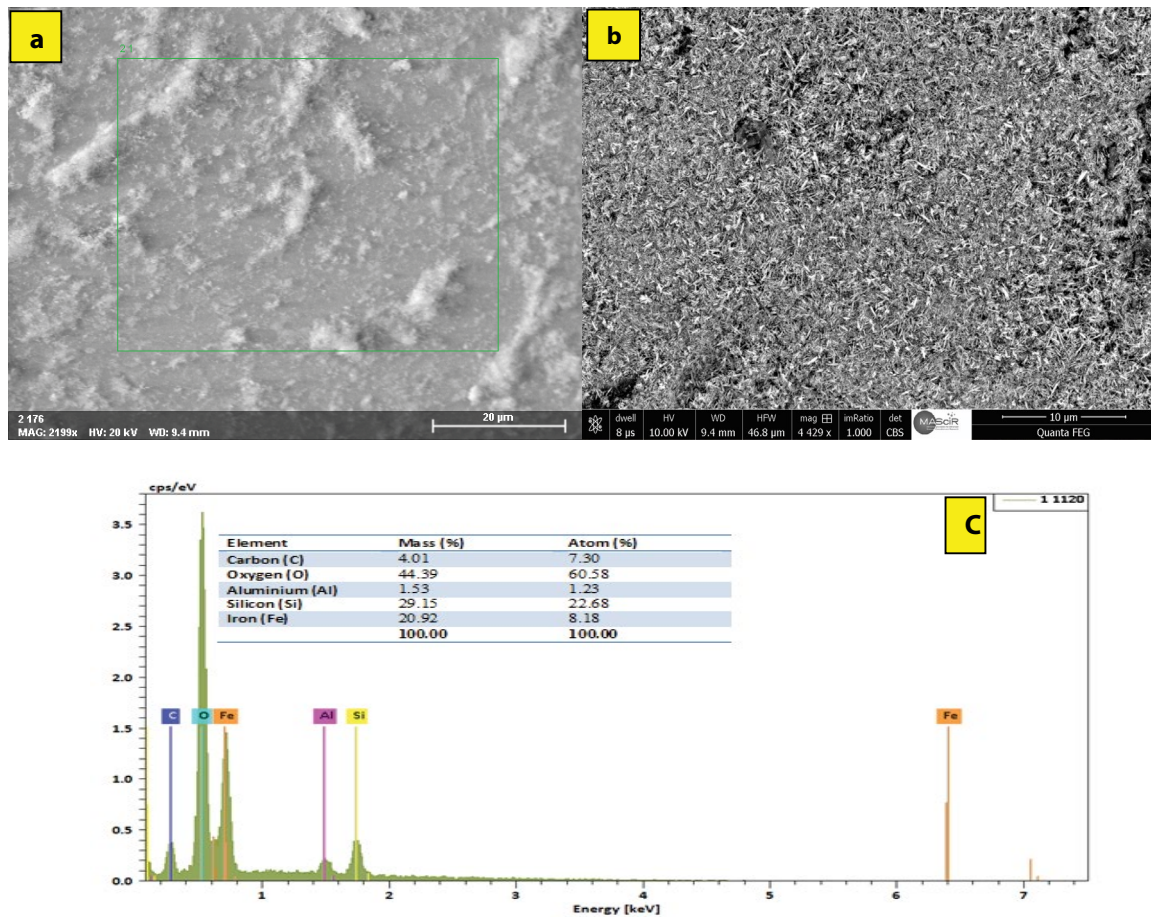- The band at 1,629 and ~3,400 cm⁻¹ corresponds to physisorbed water.

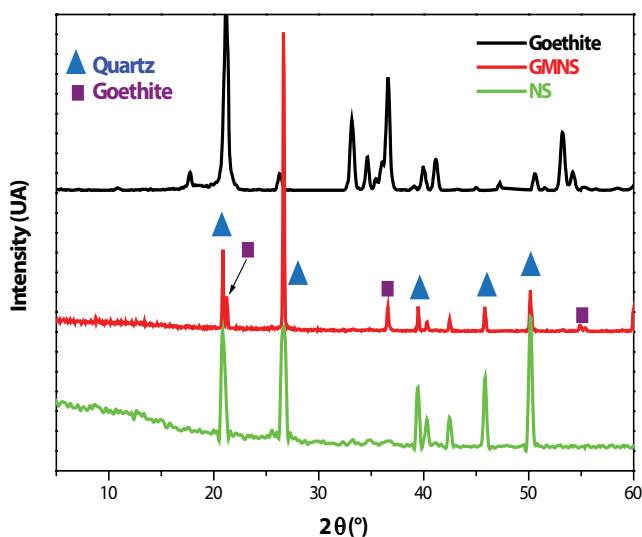Fig. 2. (a and b) SEM images of GMNS and (c) EDAX analyzes of GMNS.

Fig. 3. XRD spectra of Goethite, NS, and GMNS.

- 470 and 800 cm^{-1} characteristics bands vibrations of the silica.
- Bands at 1,088 and 1,863 cm^{-1} are attributed to the Si–O–Si siloxane bond vibrations.

For the GMNS the characteristic bands at 1,382, 908 and 782 cm^{-1} assigned to the goethite bending vibration in α-FeOOH. In effect, the 908 cm^{-1} band is ascribed to Fe–O–H stretching vibrations of goethite [47,52–54].

3.2. Adsorption of 3,4 DHBA onto GMNS in a fixed-bed column

The breakthrough curves obtained are analyzed according to the previous study [55,56]. The breakthrough time (t_b) and exhaustion time (t_e) are referred to the times at which the effluent concentration of 3,4 DHBA (C) reaches about 5%, 99%, respectively, of the influent concentration (C_0).

3.2.1. Effect of pH

The breakthrough curves for the 3,4 DHBA retention at two values pHs (pH = 5 and pH = 9) by the GMNS are presented in Fig. 5 the initial concentration of an organic molecule, ionic strength and the flow rate were fixed at constant values ([3,4 DHBA] = 15 mg/L, Q = 1 mL/min, I = 10^{-2} M in NaCl).

The clear observation of Fig. 5 suggests that when the pH value increases from pH = 5 to pH = 9, the breakthrough time (t_b) and the exhaustion time (t_e) decreased from 93 to 38 min and 263 to 153 min, respectively. These results show that the pH of the aqueous phase affects the adsorption of
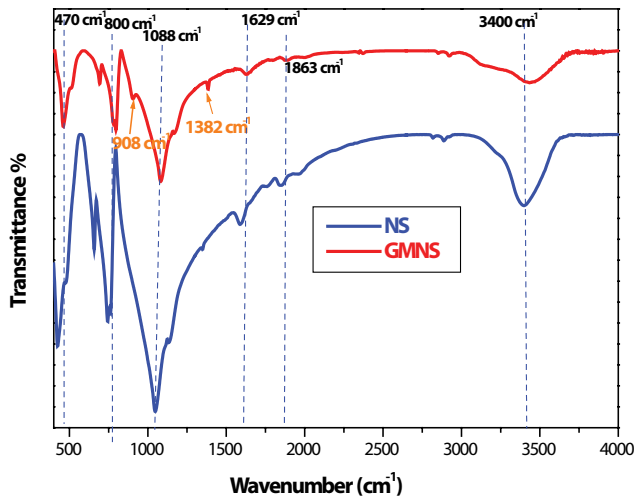
Fig. 4. FTIR of NS and GMNS.

3,4 DHBA through a column of GMNS. In fact, the estimated mass balance (Table 2) shows that the adsorbed 3,4 DHBA amount decreases from 24.31 to 10.20 mg/kg when the pH increases from 5 to 9. This behavior can be explained based on the interaction mechanism occurring between 3,4 DHBA molecule and GMNS surface.

At pH = 5, the surface of the GMNS is positively charged since it has an isoelectric point at pH of about 5.7 [5]. Further, the 3,4-DHBA molecule is negatively charged due to the deprotonation of the carboxylic group of the 3,4-DHBA (pH > pK_a (COOH) = 4.22) [57], so the electrostatic attraction occurs between the opposite charges of the adsorbent and the molecule, explaining hence the strong adsorption at this pH.

At pH = 9, (pH > pKa (–OH) and pH > IEP_{GMNS}), both the 3,4-DHBA molecule and the functional group's surface are charged negatively causing electrostatic repulsion between them. This limits the attachment of the 3,4-DHBA by GMNS surface, therefore the decrease in the amount adsorbed at basic pH. Similar results reported by Hanna et al. [58] about the adsorption of salicylic acid on natural soil.

3.2.2. Effect of initial 3,4-DHBA Concentration

The effect of initial concentration of 3,4-DHBA on their transport and adsorption by a fixed-bed column containing GMNS was examined at three 3,4-DHBA concentrations viz. 15, 40 and 60 mg/L while the other parameters were kept constant at pH = 5, Q = 1 mL/min, ionic strength $I = 10^{-2}$ M. Thus, the breakthrough curves obtained at different concentrations 15, 40 and 60 mg/L are represented in Fig. 6. It is clear from the figure that as inlet 3,4-DHBA concentration increased from 15 to 60 mg/L, both breakthrough and exhaustion times decreased from 93 to 53 min and from 263 to 115 min respectively. This may be explained by the quick saturation of the surface reactive sites at a high 3,4-DHBA inlet concentration that led to a leading to earlier the breakthrough and exhaustion times [59,60]. This result can be explained by the fact that a higher 3,4-DHBA inlet concentration leads to an earlier saturation of the surface reactive sites.

The results of the calculated mass balance are summarized in Table 2. This Table shows that an increase in the influence of 3,4-DHBA concentration from 15 to 60 mg/L. The adsorbed amount of 3,4-DHBA was found to increase from 24.31 to 35.66 mg/Kg. This can be attributed to the higher 3,4-DHBA molecule that can be available at higher concentrations, leading to a concentration gradient driving force increasing. Hence, the diffusion of the 3,4-DHBA molecules in solution towards the surface of the adsorbent increased which favorites the increase of the adsorption capacity [60,61]

3.2.3. Influence of the flow rate

To investigate the effect of flow rate on the performance of the bed column for the removal of 3,4-DHBA, the experiments were conducted at flow rates 1, 2, and 3 mL/min while keeping the influence of 3,4-DHBA concentration at 15 mg/L and pH = 5. The breakthrough curves are shown in Fig. 7. The mass balance and results from the curves are listed in Table 2. It is observed that the breakthrough time (t_b), exhaustion time (t_e) and the retention capacity decreased while the flow rate increased.

This result may be explained as following: at lower flow rate, 3,4-DHBA solution gets sufficient time for the intraparticle diffusion and mass transfer towards the GMNS surface, which increases the adsorption capacity of the column. On the contrary, at a high flow rate, the 3,4-DHBA would leave the column before the adsorption equilibrium is reached, which leads to a decrease in the efficiency of the column to eliminate 3,4-DHBA. Other researchers [5,46,60,62] have found a similar tendency.

3.2.4. Regeneration of GMNS column

The GMNS column regeneration by desorption of the 3,4-DHBA adsorbed is important for industrial applications due to the reduction of the process costs [55]. After adsorption of 3,4-DHBA onto GMNS column (pH = 5; [3,4-DHBA] = 15 mg/L and Flow rate = 1 mL/min),
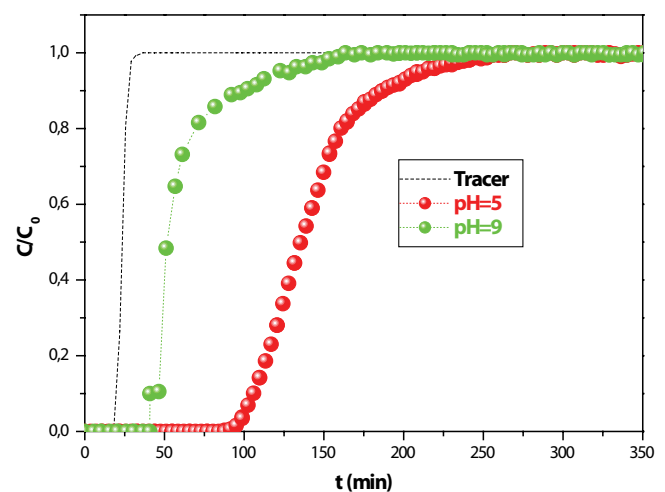

Fig. 5. Breakthrough curve of 3,4-DHBA adsorption onto GMNS in fixed-bed column at pH = 5 and 9. (Flow velocity = 1 mL/min, [3,4-DHBA] = 15 mg/L; $I = 10^{-2}$ M NaCl).

Table 2
Adsorption data for a fixed-bed column for the adsorption of 3,4-DHBA at different process parameters

Initial concentration (mg/L)	Flow rate (mL/min)	pH	t_b (min)[a]	t_e (min)[b]	q (mg/kg)[c]
15	1	5	93	263	24.31
15	1	9	38	153	10.20
15	1	5	93	263	24.31
40	1	5	60	171	30.18
60	1	5	53	106	35.66
15	1	5	93	263	24.31
15	2	5	70	200	16.9
15	3	5	45	149	11.1

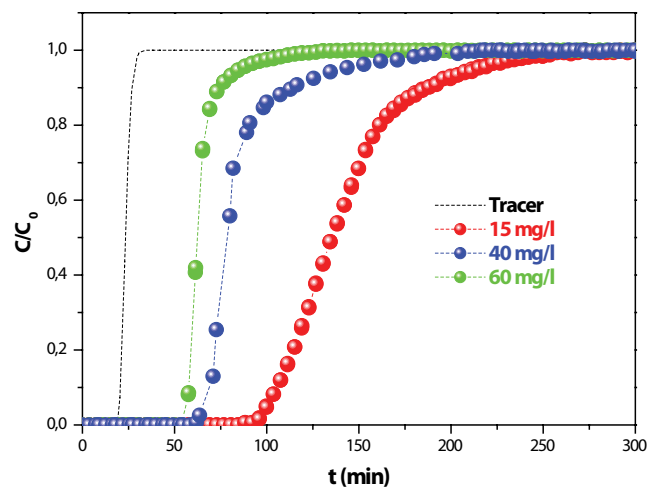[a]t_b, breakthrough time, [b]t_e, exhaustion time (t_e), and [c]q (mg/kg), amount adsorbed

Fig. 6. Breakthrough curve of 3,4-DHBA adsorption onto GMNS in a fixed-bed column at different influent concentrations. (Flow velocity = 1 mL/min; pH = 5; $I = 10^{-2}$ M).

desorption was carried with NaOH solution 0.01 M at a flow rate of 1 mL/min. Then, the GMNS column was rinsed with distilled water to remove NaOH and the regenerated column was used for the next cycle of adsorption. This cycle of adsorption–regeneration was realized for three times. The breakthrough curves obtained for the first, second and third regeneration of the 3,4-DHBA are presented in Fig. 8.

From this figure, the removal capacity of 3,4-DHBA slightly decrease at 96% for the first cycle, 91% for the second cycle and reached 83% after three consecutive of adsorption-regeneration cycle. These results show that GMNS can be used repeatedly with a slight decrease of some adsorption capacity for removal of 3,4-DHBA from solution.

3.3. Mathematical models

To describe the adsorption and transport process of organic solute in a fixed-bed column, several mathematical models can be used. In this study, two models are used such as the Yoon–Nelson and Thomas models.

3.3.1. Thomas model

The Thomas model is widely used to estimate the maximum adsorption capacity of an adsorbent, assuming the second-order reversible reaction kinetics and the Langmuir isotherm. [63].

The linearized form of the Thomas model can be expressed as Eq. (3):

$$\ln\left(\frac{C_0}{C_t} - 1\right) = \frac{k_{Th} q_{Th} m}{Q} - k_{Th} C_0 t \qquad (3)$$

where C_0 (mg/L) is the initial concentration of 3,4-DHBA, C_t (mg/L) is the outlet concentration of 3,4-DHBA at a time (min). In Eq (3) k_{Th} (mL/min mg) is the Thomas rate constant, q_{Th} is the 3,4-DHBA (mg/g) adsorbed amount of Thomas mode, m is the mass of adsorbent (g) and Q is the flow rate of solution (mL/min). The values of Thomas rate constant k_{Th} and adsorbed amount of Thomas model q_{Th} can be determined from the linear plot of $\ln[(C_0/C)-1]$ against t.

The experimental breakthrough curves for 3,4-DHBA were fitted to the Thomas model at C/C_0 ratios higher than 0.08 and lower than 0.97 [64] for flow rate and initials 3,4-DHBA concentrations. The linear plots of the Thomas model are presented in Fig. 9, the values of k_{Th}, q_{Th} and the correlation coefficients R^2 calculated from the Thomas model are listed in . The analysis of this table shows the values of q_{Th} increases with the increasing of initial 3,4-DHBA concentration, but values of k_{Th} decreased. This can be explained to the driving force between the 3,4-DHBA concentration on the adsorbent and the 3,4-DHBA in the solution [60,64,65]. Also, the Thomas rate constant, k_{Th} and maximum adsorption capacity, q_{Th} are dependent on flow rate. In effect, the increase in the flow rate from 1 to 3 ml/min results increasing of k_{Th} from 29.10^{-4} to 34.10^{-4} ml/min mg. However, although the adsorbed amount experimental and calculated q_{ex} and q_{Th} correlated weaker, the values of correlation coefficients R^2 were acceptable and ranging from 0.95 to 0.96.

3.3.2. Yoon–Nelson model

Yoon–Nelson model is a simple theoretical model based on the theory of adsorption and the breakthrough of

adsorbate probability [66]. This model is straightforward and involves less column parameters and data, and is applicable for a single component system [65,66].

The Yoon–Nelson equation, a linearized model for a single component system is expressed as Eq. (4):

$$\ln \frac{C_t}{C_0 - C_t} = k_{YN}t - \tau k_{YN} \qquad (4)$$

where k_{YN} (min^{-1}) is the rate constant, τ (min) is the time required for 50% adsorbate breakthrough. A linear plot of $\ln[C/(C_0-C)]$ vs. time (t) determined values of τ and k_{YN} from the intercept and slope of the plot (Fig. 10). The values of k_{YN} and τ were at different flow rates (1, 2 and 3 mL/min) varied at different initial concentrations of 3,4-DHBA (15, 40 and 60 mg/L) summarized in Table 3. From this Table, the rate constant of Yoon–Nelson model k_{YN} increased from 41.10^{-4} to

52.10^{-4} min^{-1} when the flow rate increases from 1 to 3 mL/min, while the time at which 50% adsorbed τ was decreased from 151 to 53 min. These results can be explained by the insufficient residence time that is, 3,4-DHBA quickly flow through the column which would be consequently, the time for the intraparticle diffusion of 3,4-DHBA towards the surface of GMNS which is not sufficient. On the other hand, when increasing initial 3,4-DHBA concentration (15 to 60 mg/L) the values of k_{YN} increased proportionally from 41.10^{-4} to 62.10^{-4} min^{-1} and led to drastic declines of τ values from 151 to 40 min due to the adsorption sites being occupied earlier by 3,4-DHBA molecules [67]. The data in Table 3 also indicate that values of τ calculated are close to the experimental results τ_{exp}.

It appears that Yoon–Nelson model is more appropriate to predict that the performance of 3,4-DHBA adsorption, by GMNS column fixed-bed. Similar observations have been
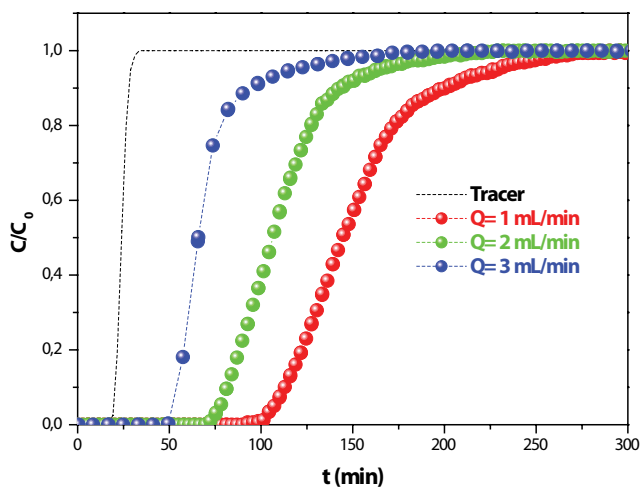

Fig. 7. Breakthrough curve of 3,4-DHBA adsorption onto GMNS in a fixed-bed column at different influent concentrations. ([3,4-DHBA] = 15 mg/L; pH = 5; $I = 10^{-2}$ M.
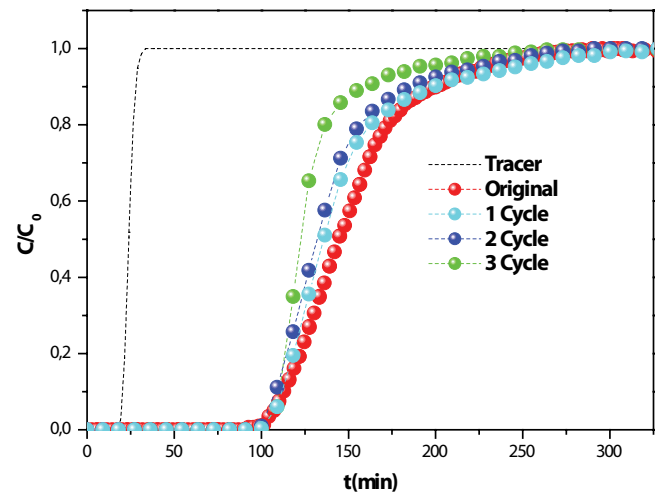
Fig. 8. Breakthrough curve for adsorption 3,4-DHBA during three adsorption-regeneration cycles. ([3,4-DHBA] = 15 mg/L; Flow velocity = 1 mL/min; pH = 5).
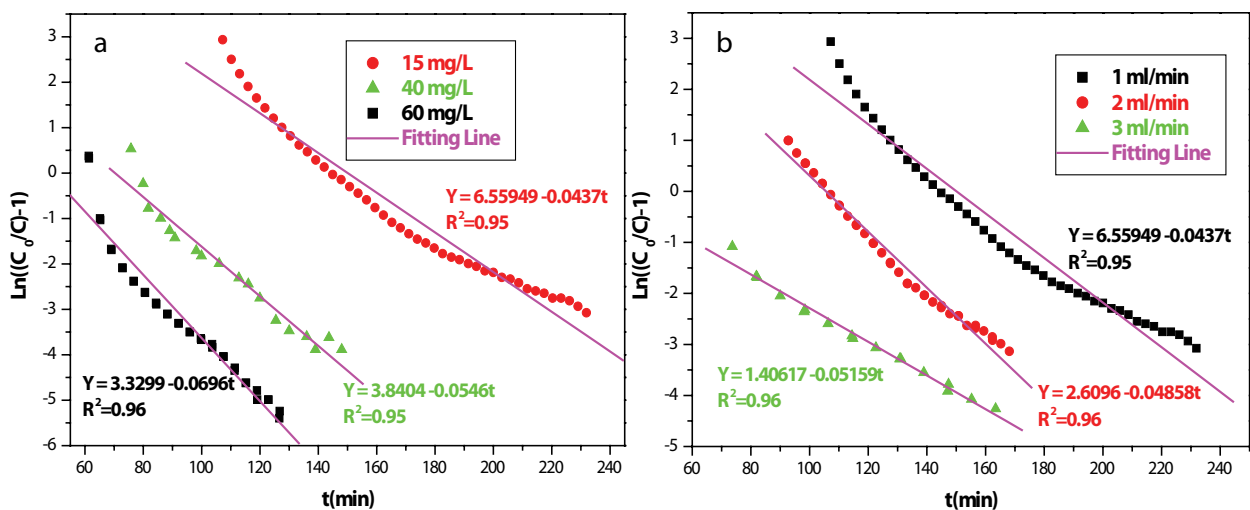

Fig. 9. The linear fitting of $\ln((C_0/C)-1)$ against t of Thomson model for 3,4-DHBA at pH = 5. (a) Effect of initial concentration and (b) Effect of flow rate.

reported in the literature. For example, Nazari et al. [60], have also found that Yoon–Nelson model is suitable for predicting the uptake capacity of cephalexin antibiotic adsorption by a column packed with walnut shell-based activated carbon.

3.4. The mechanism of 3,4-DHBA adsorption onto GMNS surface

Fig. 11 reports the FTIR of the GMNS before and after adsorption of 3,4-DHBA. Further, by comparing FTIR spectra, news peaks were observed after the adsorption of 3,4-DHBA on the GMNS, occurring at 1,313 cm^{-1} which is due to C–O stretching of benzene ring [68,69], and also occurring at the bands 1,419 and 1,620 cm^{-1} which are due to vibrations of the aromatic ring C–C, and C=C aromatic groups,

respectively, [68–70]. This appearance of the new peaks gives direct proof of the attachment of the 3,4-DHBA to the surface of the adsorbent. Also, a new peak appears at 1,539 cm^{-1} due to the carboxylic acid functional group (–COO) [69]. The appearance of the band characteristic of the –COO functional group in the FTIR spectrum after adsorption suggests that this group is not involved in the adsorption of 3,4-DHBA onto the GMNS surface. The absence of the characteristics peaks of the phenolic groups (–OH) indicates that the adsorption of 3,4-DHBA on the surface can be achieved through two adjacent OH groups by ligand exchange mechanism [70], or by the formation of the hydrogen bond between these groups and the active sites of the surface. A similar case has been reported for the adsorption of phenolic acid (3,4,5-Trihydroxybenzoic acid) on titanium dioxide TiO_2: the
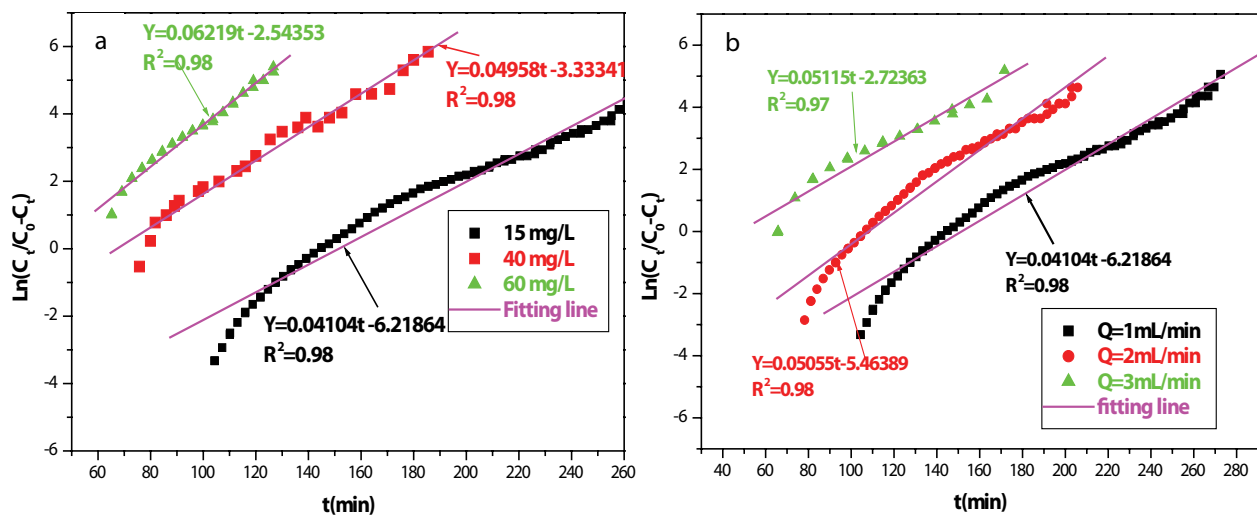

Fig. 10. The linear fitting of $\ln[C/(C_0-C)]$ against t of Yoon–Nelson model for 3,4-DHBA at pH = 5. (a) Effect of initial concentration and (b) Effect of flow rate.

Table 3
Parameters predicted by the Yoon–Nelson model, and Thomson model at different flow rates and initial concentrations

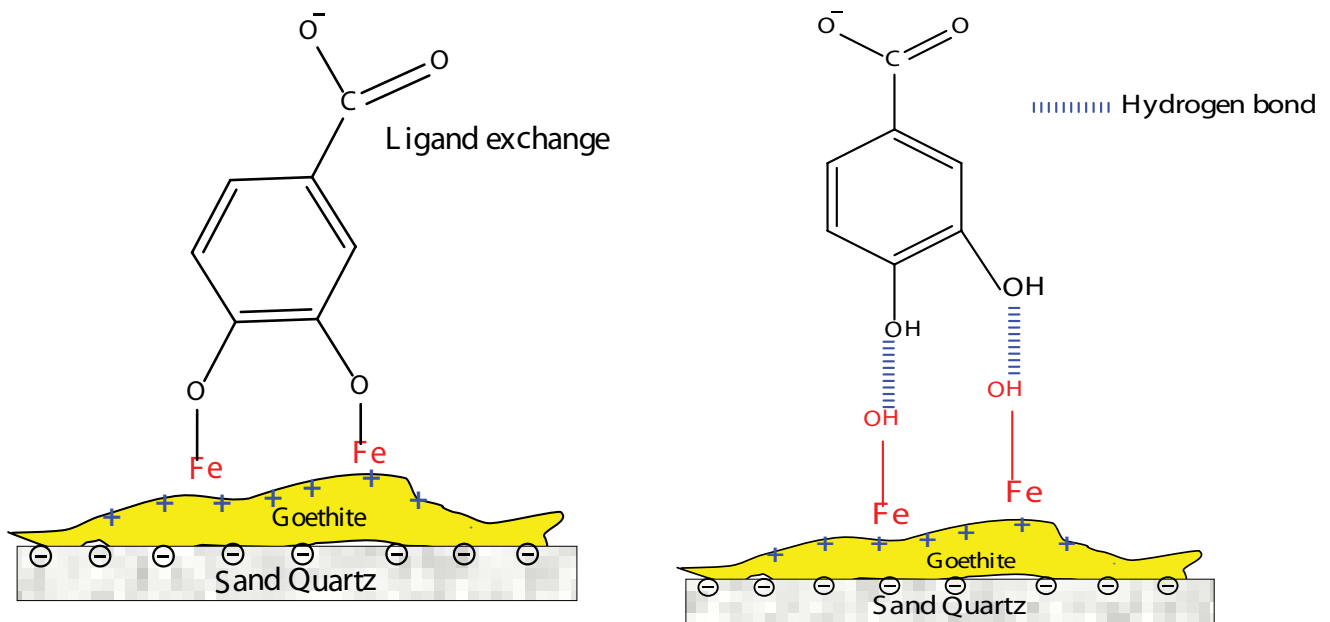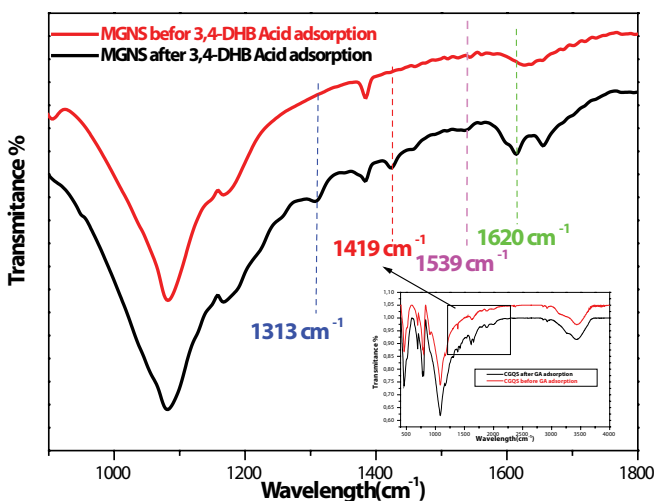| Thomas model						
C_0 (mg/L)	pH	Q (mL/min)	k_{Th} (mL/min mg) × 10^{-4}	q_{Th} (mg/kg)	q_{ex} (mg/kg)	R^2
15	5	1	29	30.8	24.3	0.95
15	5	2	32	22.3	16.9	0.96
15	5	3	34	16.79	11.1	0.96
15	5	1	29.1	30.8	24.3	0.95
40	5	1	13.7	38.39	30.18	0.95
60	5	1	11.6	39.54	35.6	0.96
Yoon–Nelson model						
C_0 (mg/L)	pH	Q (mL/min)	k_{YN} (min^{-1}) × 10^{-4}	τ (min)	τ_{exp} (min)	R^2
		1	41	151	144	0.98
15	5	2	50	109	109.9	0.98
		3	52	53	64	0.97
15			41	151	144	0.98
40	5	1	49	67	78	0.98
60			62	40	62	0.98

Fig. 12. Proposed adsorption mechanism.

Fig. 11. FTIR spectra of GMNS after and before 3,4-DHBA adsorption

interaction with the surface takes place through hydroxyls groups –OH, and the band of carboxylate group is free and appears to FTIR of TiO$_2$ after adsorption of phenolic acid [2]. Fig. 12 shows the proposed model of 3,4-DHBA adsorption onto GMNS.

4. Conclusion

In this work, natural sand modified with goethite was prepared by direct contact technique. The modified goethite natural sand obtained has been used for removal of the 3,4-DHBA in a fixed-bed column at different experimental conditions. The experimental results show that the pH, the flow rate and the initial 3,4-DHBA concentration, affect the fixed-bed column performance. The breakthrough time t_b, exhaustion time t_e and amount adsorbed of the fixed-bed column decreased on increasing the rate flow and pH, but the adsorbed amount increasing with increasing of initial 3,4-DHBA concentration. Mathematical models of Thomas and Yoon–Nelson for the breakthrough curves were applied. Yoon–Nelson model best fitted the experimental data with correlation coefficient R^2 range (0.97–0.98). The FTIR results before and after adsorption show that the adsorption of 3,4-DHBA onto the natural sand coated with goethite can be achieved through the hydroxyl groups –OH of the molecule and the active sites of the surface. Thus, GMNS can be used as a promising adsorbent for treatment contaminated water the 3,4-DHBA because of its convenience preparation by naturally available minerals.

References

[1] E. Giannakopoulos, K.C. Christoforidis, A. Tsipis, M. Jerzy-kiewicz, Y. Deligiannakis, Influence of Pb (II) on the radical properties of humic substances and model compounds, J. Phys. Chem. A, 109 (2005) 2223–2232.
[2] P.Z. Araujo, P.J. Morando, M.A. Blesa, Interaction of catechol and gallic acid with titanium dioxide in aqueous suspensions. 1. Equilibrium studies, Langmuir, 21 (2005) 3470–3474.
[3] N. Quici, M.I. Litter, A.M. Braun, E. Oliveros, Vacuum-UV-photolysis of aqueous solutions of citric and gallic acids, J. Photochem. Photobiol., A, 197 (2008) 306–312.
[4] F.F. Liu, S.G. Wang, J.L. Fan, G.H. Ma, Adsorption of natural organic matter surrogates from aqueous solution by multiwall carbon nanotubes, J. Phys. Chem. C, 116 (2012) 25783–25789.
[5] H. Ouachtak, S. Akhouairi, A.A. Addi, R.A. Akbour, A. Jada, J. Douch, M. Hamdani, Mobility and retention of phenolic acids through a goethite-coated quartz sand column, Colloids Surf., A, 546 (2018) 9–19.
[6] X. Guan, S. Yan, Z. Xu, H. Fan, Gallic acid-conjugated iron oxide nanocomposite: an efficient, separable, and reusable adsorbent for remediation of Al (III)-contaminated tannery wastewater, J. Environ. Chem. Eng., 5 (2017) 479–487.

[7]   D. Guo, Z. Zhang, D. Liu, H. Zheng, H. Chen, K. Chen, A comparative study on the degradation of gallic acid by *Aspergillus oryzae* and *Phanerochaete chrysosporium*, Water Sci. Technol., 70 (2014) 175–181.

[8]   N. Saikia, J. Sarma, J.M. Borah, S. Mahiuddin, Adsorption of 3, 4-dihydroxybenzoic acid onto hematite surface in aqueous medium: importance of position of phenolic–OH groups and understanding of the same using catechol as an auxiliary model, J. Colloid Interface Sci., 398 (2013) 227–233.

[9]   B. Cagnon, O. Chedeville, J.F. Cherrier, V. Caqueret, C. Porte, Evolution of adsorption kinetics and isotherms of gallic acid on an activated carbon oxidized by ozone: comparison to the raw material, J. Taiwan Inst. Chem. Eng., 42 (2011) 996–1003.

[10] F. Han, C. Xu, W.Z. Sun, S.T. Yu, M. Xian, Effective removal of salicylic and gallic acids from single component and impurity-containing systems using an isatin-modified adsorption resin, RSC Adv., 7 (2017) 23164–23175.

[11] J.J. Rook, Formation of haloforms during chlorination of natural waters, J. Water Treat. Exam., 23 (1974) 234–243.

[12] E. Utrera-Hidalgo, C. Moreno-Castilla, J. Rivera-Utrilla, M.A. Ferro-García, F. Carrasco-Marín, Activated carbon columns as adsorbents of gallic acid from aqueous solutions: effect of the presence of different electrolytes, Carbon., 30 (1992) 107–111.

[13] J. Wang, A. Li, L. Xu, Y. Zhou, Adsorption of tannic and gallic acids on a new polymeric adsorbent and the effect of Cu (II) on their removal, J. Hazard. Mater., 169 (2009) 794–800.

[14] M. Goyal, R. Dhawan, M. Bhagat, Adsorption of gallic acid from aqueous solution using fixed-bed activated carbon columns, Sep. Sci. Technol., 45 (2010) 1265–1274.

[15] H. Ouachtak, R.A. Akbour, A. Jada, J. Douch, A.A. Addi, M. Hamdani, Mobility of trihydroxybenzene compounds through natural quartz sand: effect of hydroxyl groups positions, J. Colloid. Sci. Biotechnol., 5 (2016) 173–181.

[16] W.W Tang, G.M. Zeng, J.L. Gong, J. Liang, P. Xu, C. Zhang, B.B. Huang, Impact of humic/fulvic acid on the removal of heavy metals from aqueous solutions using nanomaterials, a review, Sci. Total Environ., 468 (2014) 1014–1027.

[17] A.E. Fazary, E. Hernowo, A.E. Angkawijaya, T.C. Chou, C.H. Lin, M. Taha, Y.H. Ju, Complex formation between ferric (III), chromium (III), and cupric (II) metal ions and (O, N) and (O, O) donor ligands with biological relevance in aqueous solution, J. Solution Chem., 40 (2011) 1965–1986.

[18] F.J. Beltràn, J.M. Encinar, J.F. Garacia-Araya, Oxidation by ozone and chlorine dioxide of two distillery wastewater contaminants: gallic acid and epicatechin, Water Res., 27 (1993) 1023–1032.

[19] M. Panizza, G. Cerisola, Electrochemical degradation of gallic acid on a BDD anode, Chemosphere, 77 (2009) 1060–1064.

[20] L. Khaouane, Y. Ammi, S. Hanini, Modeling the retention of organic compounds by nanofiltration and reverse osmosis membranes using bootstrap aggregated neural networks, Arabian. J. Sci. Eng., 42 (2017) 1443–1453.

[21] D.P. Zagklis, A.I. Vavouraki, M.E. Kornaros, C.A. Paraskeva, Purification of olive mill wastewater phenols through membrane filtration and resin adsorption/desorption, J. Hazard. Mater., 285 (2015) 69–76.

[22] Z. Borneman, V. Gökmen, H.H. Nijhuis, Selective removal of polyphenols and brown color in apple juices using PES/PVP membranes in a single ultrafiltration process, Sep. Purif. Technol., 22 (2001) 53–61.

[23] D. Gumy, A.G. Rincon, R. Hajdu, C. Pulgarin, Solar photocatalysis for detoxification and disinfection of water: different types of suspended and fixed TiO₂ catalysts study, Sol. Energy, 80 (2006) 1376–1381.

[24] A.M. Silva, E. Nouli, N.P. Xekoukoulotakis, D. Mantzavinos, Effect of key operating parameters on phenols degradation during H₂O₂-assisted TiO₂ photocatalytic treatment of simulated and actual olive mill wastewaters, Appl. Catal., B, 73 (2007) 11–22.

[25] E. Lefebvre, B. Legube, Coagulation-floculation par le chlorure ferrique de quelques acides organiques et phenols en solution aqueuse, Water Res., 27 (1993) 433–447.

[26] P.C. Papaphilippou, C. Yiannapas, M. Politi, V.M. Daskalaki, C. Michael, N. Kalogerakis, D. Fatta-Kassinos, Sequential coagulation–flocculation, solvent extraction and photo-Fenton oxidation for the valorization and treatment of olive mill effluent, Chem. Eng. J., 224 (2013) 82–88.

[27] M. Mahdavi, M.M. Amin, Y. Hajizadeh, H. Farrokhzadeh, A. Ebrahimi, Removal of different NOM fractions from spent filter backwash water by polyaluminum ferric chloride and ferric chloride, Arabian. J. Sci. Eng., 42 (2017) 1497–1504.

[28] H.C. Kim, S.J. Park, C.G. Lee, Y.U. Han, J.A. Park, S.B. Kim, Humic acid removal from water by iron-coated sand: a column experiment, Environ. Eng. Res., 14 (2009) 41–47.

[29] A. Genz, B. Baumgarten, M. Goernitz, M. Jekel, NOM removal by adsorption onto granular ferric hydroxide: equilibrium, kinetics, filter and regeneration studies, Water Res., 42 (2008) 238–248.

[30] R.A. Akbour, H. Ouachtak, A. Jada, S. Akhouairi, A.A. Addi, J. Douch, M. Hamdani, Humic acid covered alumina as adsorbent for the removal of organic dye from colored effluents, Desal. Water Treat., 112 (2018) 207–217.

[31] C. Dong, W. Chen, C. Liu, Y. Liu, H. Liu, Synthesis of magnetic chitosan nanoparticle and its adsorption property for humic acid from aqueous solution, Colloids Surf., A, 446 (2014) 179–189.

[32] H. Ouachtak, R.A. Akbour, J. Douch, A. Jada, M. Hamdani, Removal from water and adsorption onto natural quartz sand of hydroquinone, J. Encapsulation Adsorpt. Sci., 5 (2015) 131–143.

[33] A. Bhatnagar, M. Sillanpää, Removal of natural organic matter (NOM) and its constituents from water by adsorption, A review, Chemosphere, 166 (2017) 497–510.

[34] Z. Zhang, Q. Pang, M. Li, H. Zheng, H. Chen, K. Chen, Optimization of the condition for adsorption of gallic acid by *Aspergillus oryzae mycelia* using Box–Behnken design, Environ. Sci. Pollut. Res., 22 (2015) 1085–1094.

[35] M.Y. Chang, R.S. Juang, Adsorption of tannic acid, humic acid, and dyes from water using the composite of chitosan and activated clay, J. Colloid Interface Sci., 278 (2004) 18–25.

[36] T.S. Anirudhan, M. Ramachandran, Adsorptive removal of tannin from aqueous solutions by cationic surfactant-modified bentonite clay, J. Colloid Interface Sci., 299 (2006) 116–124.

[37] T. Hartono, S. Wang, Q. Ma, Z. Zhu, Layer structured graphite oxide as a novel adsorbent for humic acid removal from aqueous solution, J. Colloid Interface Sci., 333 (2009) 114–119.

[38] R.D. Vidic, M.T. Suidan, Role of dissolved oxygen on the adsorptive capacity of activated carbon for synthetic and natural organic matter, Environ. Sci. Technol., 25 (1991) 1612–1618.

[39] J.F. Garcia-Araya, F.J. Beltran, P. Alvarez, F.J. Masa, Activated carbon adsorption of some phenolic compounds present in agroindustrial wastewater, Adsorption, 9 (2003) 107–115.

[40] K.H. Choo, S.K. Kang, Removal of residual organic matter from secondary effluent by iron oxides adsorption, Desalination, 154 (2003) 139–146.

[41] X.P. Qin, F. Liu, G.C. Wang, H. Hou, F.S. Li, L.P. Wang, Fractionation of humic acid upon adsorption to goethite: batch and column studies, Chem. Eng. J., 269 (2015) 272–278.

[42] C.H. Lai, C.Y. Chen, B.L. Wei, C.W. Lee, Adsorptive characteristics of cadmium and lead on the goethite-coated sand surface, J. Environ. Sci. Health., Part A, 36 (2001) 747–763.

[43] J.L. Gong, Y.L. Zhang, Y. Jiang, G.M. Zeng, Z.H. Cui, K. Liu, C.H. Deng, Q.Y. Niu, J.H. Deng, S.Y. Huan, Continuous adsorption of Pb (II) and methylene blue by engineered graphite oxide-coated sand in fixed-bed column, Appl. Surf. Sci., 330 (2015) 148–157.

[44] D. Dong, X. Hua, Y. Li, J. Zhang, D. Yan, Cd adsorption properties of components in different freshwater surface coatings: the important role of ferromanganese oxides, Environ. Sci. Technol., 37 (2003) 4106–4112.

[45] N. Boujelben, J. Bouzid, Z. Elouear, Studies of lead retention from aqueous solutions using iron-oxide-coated sorbents, Environ. Technol., 30 (2009) 737–746.

[46] R.A. Akbour, H. Amal, A. Ait Addi, J. Douch, A. Jada, M. Hamdani, Transport and retention of humic acid through natural quartz sand: influence of the ionic strength and the nature of divalent cation, Colloids Surf., A, 436 (2013) 589–598.

[47] A. Scheidegger, M. Borkovec, H. Sticher, Coating of silica sand with goethite: preparation and analytical identification, Geoderma, 58 (1993) 43–65.

[48] Y. Xu, L. Axe, Synthesis and characterization of iron oxide-coated silica and its effect on metal adsorption, J. Colloid Interface Sci., 282 (2005) 11–19.

[49] B. Rusch, K. Hanna, B. Humbert, Coating of quartz silica with iron oxides: Characterization and surface reactivity of iron coating phases, Colloids Surf., A, 353 (2010) 172–180.

[50] Y.S. Hwang, J.J. Lenhart, Dicarboxylic acid transport through hematite-coated sand, Chemosphere, 78 (2010) 1049–1055.

[51] T. Tosco, J. Bosch, R.U. Meckenstock, R. Sethi, Transport of ferrihydrite nanoparticles in saturated porous media: role of ionic strength and flow rate, Environ. Sci. Technol., 46 (2012) 4008–4015.

[52] R. El Haouti, H. Ouachtak, A. El Guerdaoui, A. Amedlous, E. Amaterz, R. Haounati, A. Ait Addi, N. El Alem, M.L. Taha, Cationic dyes adsorption by Na-Montmorillonite Nano Clay: experimental study combined with a theoretical investigation using DFT-based descriptors and molecular dynamics simulations, J. Mol. Liq., 290 (2019) 111139.

[53] H.D. Ruan, R.L. Frost, J.T. Kloprogge, L. Duong, Infrared spectroscopy of goethite dehydroxylation: III. FT-IR microscopy of in situ study of the thermal transformation of goethite to hematite, Spectrochim. Acta, Part A, 58 (2002) 967–981.

[54] A. Davantès, G. Lefèvre, In situ characterization of (poly) molybdate and (poly) tungstate ions sorbed onto iron (hydr) oxides by ATR-FTIR spectroscopy, Eur. Phys. J. Spec. Top., 224 (2015) 1977–1983.

[55] M.L.G. Vieira, V.M. Esquerdo, L.R. Nobre, G.L. Dotto, L.A.A. Pinto, Glass beads coated with chitosan for the food azo dyes adsorption in a fixed-bed column, J. Ind. Eng. Chem., 20 (2014) 3387–3393.

[56] A.A. Ahmad, B.H. Hameed, Fixed-bed adsorption of reactive azo dye onto granular activated carbon prepared from waste, J. Hazard. Mater., 175 (2010) 298–303.

[57] Y. Wu, K. Zhou, S. Dong, W. Yu, H. Zhang, Recovery of gallic acid from gallic acid processing wastewater, Environ. Technol., 36 (2015) 661–666.

[58] K. Hanna, L. Lassabatere, B. Bechet, Transport of two naphthoic acids and salicylic acid in soil: experimental study and empirical modeling, Water Res., 46 (2012) 4457–4467.

[59] X. Yang, Z. Shi, L. Liu, Adsorption of Sb (III) from aqueous solution by QFGO particles in batch and fixed-bed systems, Chem. Eng. J., 260 (2015) 444–453.

[60] G. Nazari, H. Abolghasemi, M. Esmaieli, E.S. Pouya, Aqueous phase adsorption of cephalexin by walnut shell-based activated carbon: a fixed-bed column study, Appl. Surf. Sci., 375 (2016) 144–153.

[61] F.J. García-Mateos, R. Ruiz-Rosas, M.D. Marqués, L.M. Cotoruelo, J. Rodríguez-Mirasol, T. Cordero, Removal of paracetamol on biomass-derived activated carbon: modeling the fixed-bed breakthrough curves using batch adsorption experiments, Chem. Eng. J., 279 (2015) 18–30.

[62] S. Akhouairi, H. Ouachtak, A.A. Addi, A. Jada, J. Douch, Natural sawdust as adsorbent for the eriochrome black t dye removal from aqueous solution, Water Air Soil Pollut., 230 (2019) 181.

[63] H.C. Thomas, Heterogeneous ion exchange in a flowing system, J. Am. Chem. Soc., 66 (1944) 1664–1666.

[64] Z. Aksu, F. Gönen, Biosorption of phenol by immobilized activated sludge in a continuous packed bed: prediction of breakthrough curves, Process Biochem., 39 (2004) 599–613.

[65] A.P. Lim, A.Z. Aris, Continuous fixed-bed column study and adsorption modeling: removal of cadmium (II) and lead (II) ions in aqueous solution by dead calcareous skeletons, Biochem. Eng. J., 87 (2014) 50–61.

[66] Y.H. Yoon, J.H. Nelson, Application of gas adsorption kinetics I. A theoretical model for respirator cartridge service life, Am. Ind. Hyg. Assoc. J., 45 (1984) 509–516.

[67] T. Ataei-Germi, A. Nematollahzadeh, Bimodal porous silica microspheres decorated with polydopamine nanoparticles for the adsorption of methylene blue in fixed-bed columns, J. Colloid Interface Sci., 470 (2016) 172–182.

[68] M. Rabiei, H. Sabahi, A.H. Rezayan, Gallic acid-loaded montmorillonite nanostructure as a new controlled release system, Appl. Clay Sci., 119 (2016) 236–242.

[69] I.Y. Tóth, M. Szekeres, R. Turcu, S. Sáringer, E. Illés, D. Nesztor, E. Tombácz, Mechanism of in situ surface polymerization of gallic acid in an environmental-inspired preparation of carboxylated core–shell magnetite nanoparticles, Langmuir, 30 (2014) 15451–15461.

[70] I.A. Jankovic, Z.V. Saponjic, M.I. Comor, J.M. Nedeljković, Surface modification of colloidal TiO_2 nanoparticles with bidentate benzene derivatives, J. Phys. Chem. C, 113 (2009) 12645–12652.